Research Article

Efficient Removal of Basic Fuchsin from Synthetic Medical Wastewater and Competitive Adsorption in the Mixture

Harez Ahmed [ID],[1] **Kareem Salihi,**[1] **Stephan Kaufhold,**[2] **Bakhtyar Aziz** [ID],[3] **Musa Hama Radha,**[1] **Lava Karim,**[1] **and Hevi Nooralddin**[1]

[1]*Department of Chemistry, College of Science, University of Sulaimani, Sulaimanyah, Iraq 46001*
[2]*Federal Institute for Geosciences and Natural Resources (BGR), Stilleweg 2, 30655 Hannover, Germany*
[3]*Department of Nano-Science and Applied Chemistry, College of Medical and Applied Sciences, Charmo University, Chamchamal, Iraq 46023*

Correspondence should be addressed to Harez Ahmed; harez.ahmed@univsul.edu.iq

The Ziehl-Neelsen stain is a mixture of Basic Fuchsin (BF), phenol (Ph), and methylene blue. It is used to stain the cell walls of Mycobacterium species. In this study, Basic Fuchsin was efficiently removed from synthetic wastewater using natural clay of Gankawa (GC) from Sulaimanyah city, and the effect of the presence of high concentrations of phenol in the adsorption mixture is demonstrated. In addition, X-ray diffraction (XRD), X-ray fluorescence (XRF), N_2 gas adsorption analyzer, and field-emission scanning electron microscopy (FESEM) were used to characterize the natural clay. The clay was found to be mostly calcite, with a minor percentage of smectite, and contaminated with low percentages of illite. The adsorption kinetics show a relatively fast equilibration time (60-70 minutes). A second-order pseudokinetic model better fits the experimental kinetic data. The effect of the initial pH of the solution mixture was negligible at the experimental concentration range of the study. Freundlich and Langmuir's adsorption isotherm models were applied to the equilibrium experimental data using nonlinear regression curve fitting. Both kinetics and isotherm studies point to a chemical adsorption mechanism for the process. For adsorption in the mixture, phenol molecules were found to compete with BF molecules for the active adsorption sites, while a synergetic effect of BF exists on phenol adsorption. As a naturally abundant cheap material, GC shows a superior adsorption capacity toward BF ($287.0 \, \mathrm{mg \, g^{-1}}$) over all natural materials and most of the synthetic or modified materials found in the literature.

1. Introduction

Dyes are one of the largest water pollutants worldwide [1]. On a large scale, dyes enter water and wastewater either directly from the dye manufacturing industry or from the finishing steps in coloring other industrial products such as textiles, cosmetics, leather, food, and paper [2]. In addition to their effect on increasing the biochemical oxygen demand by preventing light penetration in aquatic systems which is essential for photosynthesis, most synthetic dyes are toxic [3], mutagenic, and carcinogenic [4] and cause detrimental effects on the water environment if not removed from effluents before entering the ecosystem. Several dyes are used by clinical laboratories to colorize bacteria to give better

resolution under the microscope. Because it is straightforward and inexpensive, the Ziehl-Neelsen method is frequently employed for coloring sputum smears in underdeveloped nations [5]. To accelerate the rate of the formation of the mycolate-fuchsin complex in the cell wall, BF solution is applied to the specimen and heated. A counterstain, such as 0.3% methylene blue, is then applied and the acid-fast bacteria are colored red-violet on a blue background to be visualized under microscopes [6, 7]. The excess of the stain in all blood film preparation methods goes to sewage via the washing steps of the slide preparation procedures [8] unless it is collected separately. Medical laboratory effluents have other disadvantages and lead to several water problems, such as taste, odor, color, turbidity, and pH. The

biotransformation products of organic molecules, such as dyes, adversely affect human health because of their toxicity and carcinogenic and mutagenic effects even if they are present in trace amounts [9, 10]. A variety of technologies are available for removing synthetic dyes from water and wastewater to reduce their environmental impacts, such as sedimentation, filtration technology, oxidation, membrane isolation, electrocoagulation, advanced activated process, biodegradation, adsorption, and ion exchange [11, 12]. To remove these toxic materials from effluent streams, adsorption technology remains the best choice because of its simplicity and cost-effectiveness [13]. Among the huge sources of absorbents, recent investigations focused on the effectiveness of low-cost adsorbents for dye removal such as rice husk carbon [14], walnut shell powder [15], sawdust [16], sewage sludge [17], activated clay [18], chitosan [19], and agricultural waste [20]. Novel materials are growing attention for diverse uses based on their specific functionality and surface area as reported by the Awual group where they used a ligand-based composite material for the detection and removal of metal ions at trace levels with 100% regeneration and reuse [21–23]. Such materials may be useful for removing trace amounts of metal ions only and for limited water effluents, because of their higher cost than naturally abundant adsorbent sources like clay. Even though activated carbon has the highest adsorption capacity for the adsorption of organic and inorganic species, due to its disadvantages (like cost and difficulties in separation and reactivation), researchers are continuously seeking cheap and more abundant adsorbents [24]. Agricultural waste [25, 26] and natural clay [27, 28] are mostly attracted materials after activated carbon. Clays are promising adsorbents because they are affordable and readily available, and they have a high capacity for the adsorption of a variety of organic and inorganic contaminants [29]. The current study was aimed at evaluating a local clay to be used as an efficient adsorbent for removing Basic Fuchsin from wastewater.

Using local source adsorbents for the treatment of dye-contaminated wastewater may be the best choice.

2. Materials and Methods

The clay from Gankawa (GC) in Sulaimanyah, Iraq, was extracted from the surface to avoid contamination of organic and agricultural plants. The fine fraction practice was separated from the clay using successive dilution and sedimentation in a 1 L cylinder. The sample was dried at 105 degrees Celsius and passed through a 200-micron sieve. Basic Fuchsin (BF) dye was purchased from JOURILABS.

The BF solutions were prepared using ethanol as a solvent. A concentration of $400 \, mg \, L^{-1}$ BF was prepared and used as a stock solution from which a series of standard concentrations were prepared by dilution with ethanol to obtain the calibration curve. A Cary 60 UV-Vis spectrophotometer from Agilent Technologies, USA, was used to measure absorbance at $\lambda_{max} = 550 \, nm$.

2.1. Adsorbent Characterization. The chemical composition of Gankawa clay (GC) was analyzed using energy-dispersive X-Ray Fluorescence (XRF) spectroscopy at the State Company

of Geological Survey and Mining of Iraq. 1000 mg of GC clay was heated to 1000°C for 1 hour to determine the loss on ignition (LOI). A PANalytical X'Pert PRO X-ray diffractometer (XRD) was used to record the XRD patterns (Cu-$K_{\alpha1}$ radiation generated at 40 kV and 30 mA). Specific surface area, pore volumes, and pore diameters were analyzed by an N_2 gas adsorption analyzer using a Micrometrics Gemini VII 2390t apparatus. The analysis was performed at 77 K. A field-emission scanning electron microscope model ZEISS SIGMA FE-SEM was used to record the surface morphology of the clay.

2.2. Adsorption Studies. The adsorption experiments were conducted using 0.2 g of GC with 25 mL of the BF solution (various concentrations) in 100 mL dark polyethylene bottles. A 120 rpm agitation rate in a thermostat water bath shaker model GFL was used for all the experiments. At specified time intervals of the adsorption process, 5 mL of the dispersions was centrifuged for 10 minutes at 5000 rpm. The remaining concentrations of the stain in the supernatants were determined by a UV-visible spectrophotometer. Equation (1) was used to calculate the amount of the adsorbed BF, qe (mg g^{-1}).

$$q_e = \left(\frac{C_o - C_e}{m} \right) \times V, \tag{1}$$

where C_o and C_e are the initial and equilibrium concentrations of the stain (mg L^{-1}), respectively, V is the volume of the mixture (L), and m is the mass of the adsorbent (g).

The equilibrium time was studied first (0 to 120 min) at room temperature; then, the effect of the initial pH of the solution mixture was studied in the range of 2 to 10 using diluted HCl and NaOH to control the initial pH. The kinetics and isotherm studies for the adsorption process were investigated at different temperatures.

2.3. Error Analysis. To resolve the theoretical kinetic and isotherm models that best fit the experimental kinetic and equilibrium data, the error analysis for the nonlinear curve fittings was performed. The correlation index (coefficient of determination) (R^2) and the sum of square errors (SSE) were calculated according to Eqs. (2) and (3), respectively, using the OriginPro software computer program.

$$R^2 = 1 - \frac{\sum \left(q_{exp} - q_{fit} \right)^2}{\sum \left(q_{exp} - q_{mean} \right)^2}, \tag{2}$$

where q_{fit} is the estimated value of q_{exp} for the model under investigation. The better fit of a model is the one with R^2 closer to 1.0.

$$SSE = \sum \left(q_{exp} - q_{fit} \right)^2. \tag{3}$$

The smaller the values of SSE, the better the fit of the model under investigation.
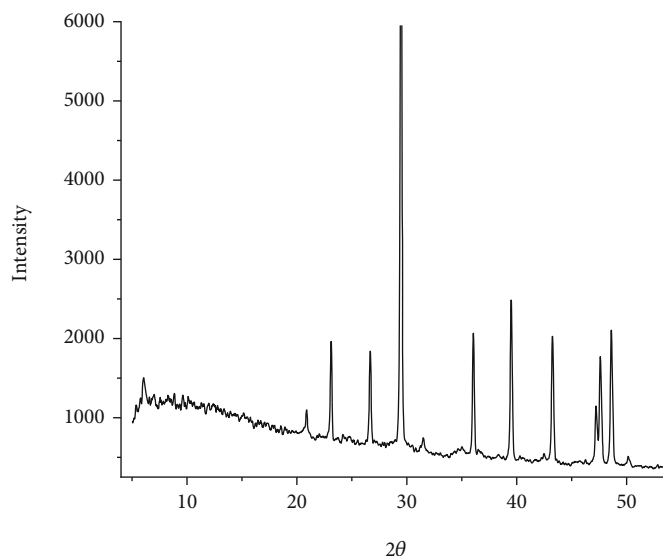
FIGURE 1: XRD pattern of the GC clay sample.

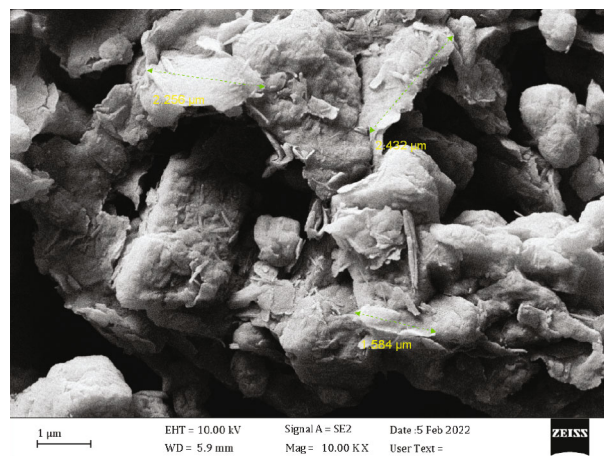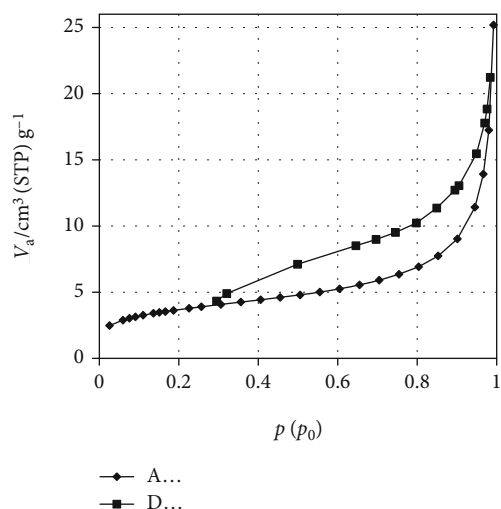FIGURE 2: N_2 gas adsorption-desorption isotherms for GC at 77 K.

FIGURE 3: FESEM micrograph for GC.

3. Results and Discussion

3.1. Adsorbent Characterization. The percentages of the components represented as their oxides were estimated to be SiO_2 (34.3%), Al_2O_3 (4.2%), Fe_2O_3 (2.4%), Na_2O (0.1%), K_2O (0.7%), CaO (38.7%), MgO (1.7%), and LOI (17.0%).

The XRD pattern of GK shows several peaks (Figure 1). The most intense peaks found at $2\theta = 23.16°$, $29.51°$, $39.52°$, $43.26°$, $47.14°$, $47.63°$, and $48.61°$ were matched to the calcite content. The peak around $36.0°$ may be assigned to calcite and/or hematite. Quartz peaks were found at $2\theta = 20.9°$ and $26.7°$. The peak at $6.1°$ belongs to smectite and/or illite clay mineral with a d-spacing of 14.48 Å. The oriented slides for normal and ethylene glycol-saturated clay (Figure S1) show a shift of the I/S peak from 14.48 Å to 17.32 Å, which points to the presence of montmorillonite.

The surface properties of the GC clay were determined from the N_2 gas adsorption-desorption isotherms at 77 K (Figure 2). The BET surface area (S_{BET}), BJH pore volume (V_P), and mean pore diameter were estimated as $13.57 \, m^2 \, g^{-1}$, $0.0368 \, cm^3 \, g^{-1}$, and 10.84 nm, respectively. The hysteresis, where the desorption isotherm appears above the adsorption isotherm, becomes noticeable at a low relative pressure ($P/P_o < 0.4$) due to the low rate of diffusion in the inner pores. This may be explained by the fact that the inner meso- and macropores were accessible mainly via the micropores [30]. The apparent SBET shows lower values than the true surface area in such cases. An aggregate of flakey grains of different particle sizes and irregular particle shapes can be seen from the FE-SEM image (Figure 3) which is expected for natural clays [31]. Illite appears as microfibers in the micrograph.

3.2. Adsorption Studies. The equilibrium time study and the effect of the initial pH of the solution for the adsorption of BF on GC are shown in Figures S2 and S3, respectively. The equilibrium time was estimated to be 60 minutes, and
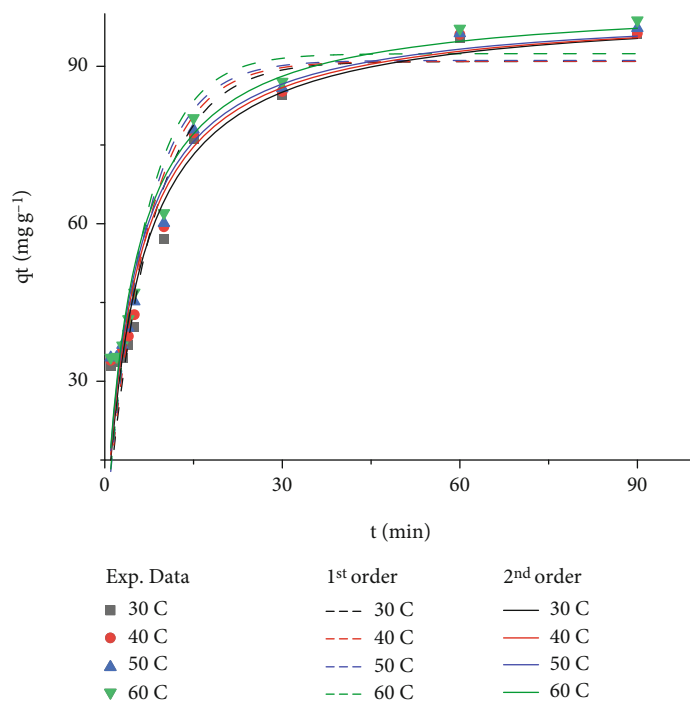
FIGURE 4: Pseudo-first-order and pseudo-second-order adsorption kinetics for BF on GC (0.2 g GC, 150 mL of 400 mg L^{-1} BF, initial pH = 6.5, stirring = 120 rpm, different temperatures).

TABLE 1: Kinetic parameters for the adsorption of BF on GC at different temperatures.

Kinetic model	Kinetic parameters	Temperature			
		303 K	313 K	323 K	333 K
First order	k_1 (min^{-1})	0.134 ± 0.026	0.144 ± 0.028	0.151 ± 0.029	0.155 ± 0.028
	q_e (mg/g)	90.9 ± 5.9	90.9 ± 5.8	91.1 ± 5.7	92.4 ± 5.5
	SSE	826.8	829.6	828.7	775.7
	R^2	0.871	0.867	0.865	0.877
Second order	k_2 (L mol^{-1} min^{-1})	$1.71 \times 10^{-3} \pm 4.4 \times 10^{-4}$	$1.87 \times 10^{-3} \pm 4.7 \times 10^{-4}$	$1.97 \times 10^{-3} \pm 4.7 \times 10^{-4}$	$1.98 \times 10^{-3} \pm 4.5 \times 10^{-4}$
	q_e (mg/g)	101.4 ± 6.3	101.1 ± 6.0	101.1 ± 5.7	102.6 ± 5.4
	SSE	513.8	495.0	464.8	426.8
	R^2	0.920	0.920	0.924	0.932

the initial pH shows no significant effect on the adsorption process.

3.2.1. Kinetics of the Adsorption. The mechanism of the adsorption of a solute on an adsorbate can be clarified via the study of the adsorption kinetics. For this purpose, different kinetic models have been proposed to deduce the rate-determining step and the controlling mechanism like mass transfer mechanism or chemical reaction. In this study, pseudo-first-order (suggested by Lagergren, Eq. (4)) [32] and pseudo-second-order (suggested by Hoo, Eq. (5)) [33] kinetic equations were applied to the experimental data, and their error analysis such as the correlation coefficient (R^2) and the sum of square errors (SSE) were compared to
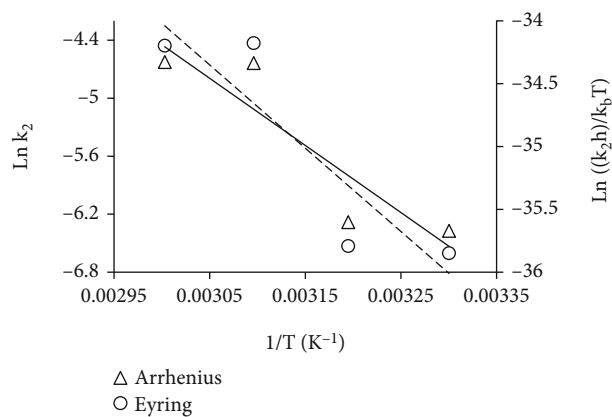

FIGURE 5: Arrhenius and Eyring plots for the adsorption of BF onto GC.

TABLE 2: Activation parameters for the adsorption of BF on GC.

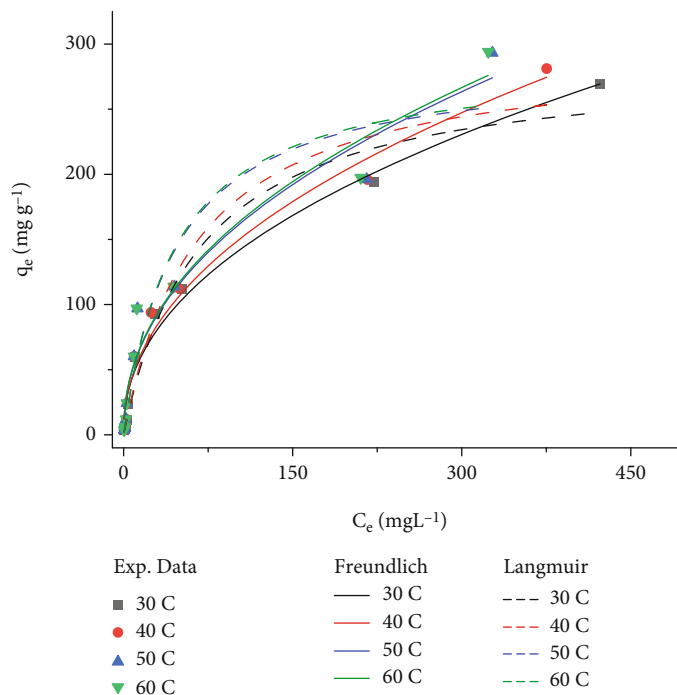| Temp. (K)	E_a (kJ mol^{-1})	ΔH^* (kJ mol^{-1})	ΔS^* (J mol^{-1})	ΔG^* (kJ mol^{-1})
303				90.7
313				91.9
323	57.7 ± 2.3	55.1 ± 2.1	-117.5 ± 7.2	93.1
333				94.2

FIGURE 6: Langmuir and Freundlich adsorption isotherms for the adsorption of BF on GC (0.2 g GC, 150 mL BF, initial pH = 6.5, stirring = 120 rpm, different temperatures).

show the fitting kinetic model.

$$q_t = q_e \left(1 - e^{k_1 t}\right), \tag{4}$$

$$q_t = \frac{k_2 q_e^2 t}{1 + k_2 q_e^2 t}, \tag{5}$$

where q_t and q_e are the amounts of dye adsorbed (mg g^{-1}) at time t (min.) and equilibrium, respectively. k_1 and k_2 are the pseudo-first-order (min^{-1}) and pseudo-second-order (g mg^{-1} min^{-1}) rate constants, respectively. The kinetics of the adsorption of BF on GC was studied at four different temperatures (303, 313, 323, and 333 K). Figure 4 shows the experimental kinetic data and the nonlinear regression curves for the applied pseudo-first-order and pseudo-second-order kinetic models on the experimental data. The estimated kinetic parameters are shown in Table 1.

The error analysis (R^2 and SSE) for the applied kinetic models on the experimental data shows the better fitting of the pseudo-second-order kinetics. At the studied range of temperature (303 to 333 K), the adsorption capacity

was not affected by temperature change, while the pseudo-second-order rate constants slightly increased with increasing temperature which may be due to the increase of the diffusion rate of the BF from the bulk solution to the surface of GC [34].

The activation parameters (E_a, ΔH^*, ΔS^*, and ΔG^*) were estimated from the slope and intercepts of Arrhenius (Eq. (6)) and Eyring (Eq. (7)) plots (Figure 5), and the parameters are tabulated in Table 2.

$$\ln k_2 = \ln A - \frac{E_a}{RT}, \tag{6}$$

$$\ln \frac{k_2 h}{k_B T} = \frac{\Delta S^*}{R} - \frac{\Delta H^*}{RT}, \tag{7}$$

where E_a is the activation energy (J mol^{-1}), A is the Arrhenius constant (g mol^{-1} s^{-1}), R is the gas constant (8.314 J K^{-1} mol^{-1}), ΔS^* is the entropy of activation (J mol^{-1}), and ΔH^* is the enthalpy of activation (kJ mol^{-1}).

Activation energies around 40-800 kJ mol^{-1} point to a chemically controlled mechanism, while below 40 kJ mol^{-1}

TABLE 3: The adsorption isotherm parameters for the adsorption of BF onto GC.

Isotherm		Temperature (K)			
Model	Parameters	303	313	323	333
Langmuir	q_m (mg g^{-1})	287.0 ± 23.3	287.1 ± 28.0	287.3 ± 34.8	$289.235.2$
	K_L (L mg^{-1})	0.0148 ± 0.0038	0.0154 ± 0.0046	0.0215 ± 0.0090	0.0217 ± 0.0091
	SSE	2048	2804	5691	5742
	R^2	0.970	0.962	0.928	0.928
Freundlich	K_F ((mg g^{-1})(L mg^{-1})$^{1/n}$)	17.33 ± 3.1	17.32 ± 3.4	19.60 ± 5.7	19.83 ± 5.7
	n	2.20 ± 0.16	2.15 ± 0.17	2.20 ± 0.27	2.19 ± 0.26
	SSE	1143	1349	3245	3188
	R^2	0.984	0.982	0.959	0.960

is assigned to a physically controlled mechanism. The E_a in this study was estimated as 57.7 kJ mol^{-1} which is attributed to a chemisorption mechanism [35].

3.2.2. Isotherms of the Adsorption. The adsorption isotherm provides information about the affinity of the adsorbent to the surface of the adsorbate at equilibrium which governs the distribution of the adsorbate between solution and adsorbent.

The monolayer adsorption of the absorbate on the adsorbent is best described by the Langmuir isotherm (Eq. (8)). The premise of an energetically identical adsorption site on a homogeneous surface and the absence of any interspecies interaction form the basis of the Langmuir isotherm [36]. This isotherm is also appropriate to determine the maximum adsorption capacity from the experimental data [37].

$$q_e = \frac{q_m K_L C_e}{1 + K_L C_e}, \tag{8}$$

where C_e is the concentration of the adsorbate (mg L^{-1}) at equilibrium, q_m is the monolayer maximum adsorption capacity of the adsorbent (mg g^{-1}), and K_L is the Langmuir adsorption constant (L mg^{-1}).

The Freundlich isotherm (Eq. (9)) was formulated for multilayer adsorption on heterogeneous surfaces [38].

$$q_e = K_f C_e^{1/n}, \tag{9}$$

where K_F [(mg g^{-1})(mg L^{-1})$^{1/n}$] is the adsorption capacity and n is the nonlinearity coefficient.

Figure 6 shows Langmuir and Freundlich adsorption isotherms for the adsorption of BF on the clay sample (GC) at 30, 40, 50, and 60°C. The estimated isotherm parameters from the graphs are listed in Table 3.

The error analysis for the adsorption isotherms shows that both Langmuir and Freundlich models are fitted well with the experimental data. The adsorption capacity (q_m) was found to be insensitive to temperature, while a slight increase in the Langmuir equilibrium constant is seen.
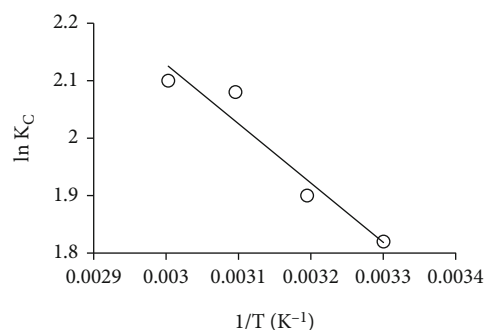

FIGURE 7: Van't Hoff plot for the adsorption of BF on GC.

3.2.3. Thermodynamic Study. The thermodynamic parameters (Gibbs free energy change $\Delta G \circ$, enthalpy change $\Delta H \circ$, and entropy change $\Delta S \circ$) from the variation of K_C with temperature using the following equations.

$$\Delta G \circ = -RT \ln K_C, \tag{10}$$

$$\Delta G \circ = \Delta H \circ - T\Delta S \circ, \tag{11}$$

$$\ln K_C = \frac{\Delta S \circ}{R} - \frac{\Delta H \circ}{RT}, \tag{12}$$

where K_C is the thermodynamic equilibrium constant for the adsorption of BF on GC. The values of K_C were estimated from the intercept of the plots of $\ln (q_e/C_e)$ vs. q_e [39] (Figure S4). The plot of $\ln K_C$ vs. $1/T$ (Figure 7) shows a straight line from which $\Delta H \circ$ and $\Delta S \circ$ were evaluated from the slope and the intercept (Table 4).

The thermodynamic parameters point to endothermic adsorption (positive value of $\Delta H \circ$). An increase in the randomness of the molecules at the solid/liquid interface is reflected by the high positive value of $\Delta S \circ$ which points to the high affinity of the GC surface to BF dye molecules. The adsorption process was spontaneous and feasible as indicated by the high negative values of $\Delta G \circ$ [40, 41].

3.2.4. Comparison of Adsorption of BF in Mixture with Phenol. The Ziehl-Neelsen stain uses BF and phenol (Ph) chemicals to stain the cell wall of Mycobacterium species,

TABLE 4: Thermodynamic parameters for the adsorption of BF on GC.

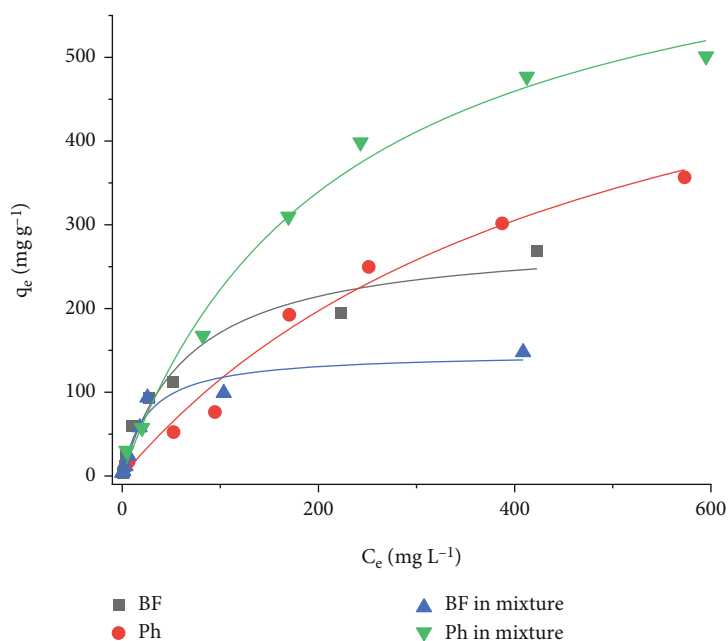| Temperature (K)	$\Delta H \circ$ (kJ mol^{-1})	$\Delta S \circ$ (J mol^{-1})	$\Delta G \circ$ (kJ mol^{-1})
303			-4.58
313			-5.02
323	8.58	43.44	-5.45
333			-5.89

FIGURE 8: Adsorption isotherms of BF and Ph separately and in the mixture.

and the washing waste would be a mixture of BF and phenol. Therefore, the adsorption of BF in a mixture with phenol was studied. First, the adsorption isotherm for phenol on GC was studied separately; then, the adsorption isotherms for BF and Ph were studied in a mixture together (Figure 8).

From the isotherms in Figure 8, competitive adsorption, on the active adsorption sites on GC, was detected for the adsorption of BF in a mixture with Ph (the adsorption capacity for BF adsorption has declined from 287.0 to 147.3 mg g^{-1}), while a synergetic effect of BF molecules was found on the adsorption of phenol on GC (the adsorption capacity of GC towards phenol molecules has increased from 675.4 to 711.6 mg g^{-1}) [42].

3.2.5. Adsorption Mechanism.
The high adsorption capacity of the clay for cationic BF dye onto the natural clay can be explained by the formation of links with anionic acid groups on the adsorbent to adhere to the clay surface, which was described in terms of a chemisorption mechanism. For the adsorption of phenol in the presence of BF, the synergetic effect may be due to the formation of hydrogen bonds between the nitrogen of the amine group of the adsorbed BF and the oxygen atoms of the phenol molecules in addition to the directly adsorbed phenol molecules by the active sites (Figure 9) [43].
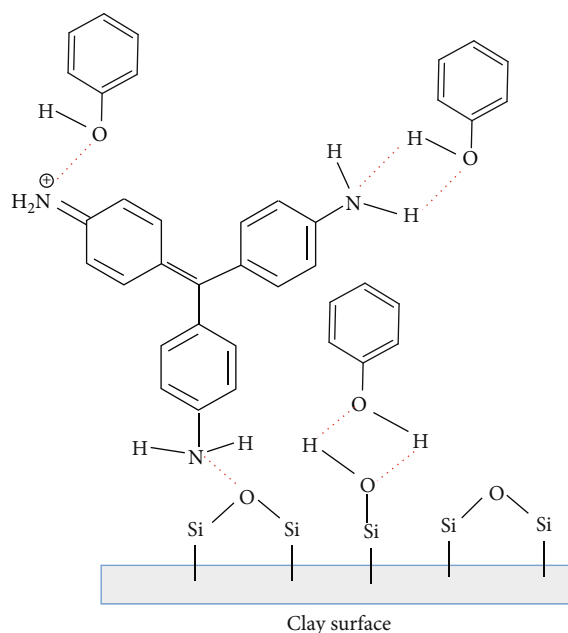

FIGURE 9: Synergetic effect on the adsorption of phenol on GC in the presence of BF.

Table 5: Comparison of the adsorption capacity of GC with other reported natural, modified, and synthetic adsorbents.

	Material used	Modification	q_m (mg g^{-1})	Reference
1	Raw pistachio nutshells	None	118.2	[44]
2	Eggshell membrane	None	48	[45]
3	Cellulose	None	124.0	
4	Cellulose-based nanocrystals	Synthetic	262.0	[46]
5	Cellulose nanocrystals	Synthetic and carboxylate-functionalized	320.0	
6	Graphene/Fe$_3$O$_4$	Synthetic	85	[47, 48]
7	Malted sorghum mash	HCl-treated	58.5	[49]
9	Diatomite	Alkali-activated	<2	[50]
10	Mussel shell	Calcined	141.6	[51]
11	Triptycene-based porous organic polymer	Synthetic (ungrafted)	188.3	[52]
		Synthetic and sulfonic-grafted	586.2	
12	Rambutan peel	Immobilized	108.6	[53]
13	Biomass of Baker's yeast	None	48.7	[54]
		Poly(amic acid)-modified	353.4	
13	Gankawa clay (GC)	None	287	Present study

3.2.6. Comparison of GC Clay with Other Natural, Modified, and Synthetic Adsorbents. The maximum monolayer adsorption capacity (q_m) of BF of various adsorbents is summarized in Table 5. The GC clay used in this research shows superior adsorption capacity over natural and modified clays in literature and comparable adsorption capacity to synthetic materials. Due to its abundance and low cost, GC clay has the advantage over other adsorbents.

4. Conclusion

In the present study, we demonstrated the high efficiency of local natural clay to adsorb the cationic dye (Basic Fuchsin) from aqueous media which was reflected by the monolayer adsorption capacity (q_m). Phenol was found to compete with BF molecules strongly for the adsorption sites, and BF has a synergetic effect on the adsorption of phenol molecules due to hydrogen bonding. The adsorption of BF on GC occurred spontaneously through an exothermic process with increasing molecular randomness on the surface of the clay particles that show the high affinity of the clay surface to the BF molecules. The adsorption follows a pseudo-second-order kinetics with an activation energy of 57.7 kJ mol^{-1} that points to a chemical adsorption process.

In the comparison of the adsorption capacity of the present natural clay to other materials, GC may be considered a promising material for application in the elimination of cationic dyes from industrial effluents.

Data Availability

The authors confirm that the data supporting the finding of this study are available within the article.

Conflicts of Interest

The authors have no conflict of interest.

Authors' Contributions

All authors contributed to the study's conception and design. Material preparation, data collection, and analysis were performed by Harez Rashid Ahmed, Musa Mohammed Hama Radha, Lava Kamal Karim Abdulla, and Hevi Ahmed Nooralddin. Clay characterization, data interpretation, and analysis were performed by Stephan Kaufhold, Bakhtyar Kamal Aziz, and Kareem Jummah Al Salihi. The first draft of the manuscript was written with the aid of Harez Rashid Ahmed, and all authors commented on previous versions of the manuscript. All authors examined and approved the very last manuscript.

Supplementary Materials

Texture slides (oriented slides) were prepared for the XRD analysis by the top loading method. One of them was stored in a closed vessel in an ethylene glycol (EG) atmosphere at 60°C overnight and the other kept normally (N). After cooling to room temperature, the two clay slides were analyzed for XRD from 2° to 40° (2θ) with a step size of 0.03° 2θ and 5 s per step. A shift of the illite (I) and/or smectite (S) peak from 14.48 Å to 17.32 Å points to the presence of montmorillonite (Figure S1). The equilibrium time for the adsorption of BF on GC was first studied (Figure S2) to be 60 minutes, and the pH study shows no significant effect of pH on the adsorption process (Figure S3). The thermodynamic equilibrium constants (K_C) for the adsorption of BF on GC at different temperatures (30, 40, 50, and 60°C) were evaluated from the intercept of Khan plots of ln (q_e/C_e) vs. q_e (Figure S4). (*Supplementary Materials*)

References

[1] H. Patel, E. Routoula, and S. V. Patwardhan, "Decontamination of anthraquinone dyes polluted water using bioinspired

silica as a sustainable sorbent," *SILICON*, vol. 14, no. 3, pp. 1235–1245, 2022.

[2] A. A. Adeyemo, I. O. Adeoye, and O. S. Bello, "Adsorption of dyes using different types of clay: a review," *Applied Water Science*, vol. 7, no. 2, pp. 543–568, 2017.

[3] D. A. Yaseen and M. Scholz, "Textile dye wastewater characteristics and constituents of synthetic effluents: a critical review," *International journal of Environmental Science and Technology*, vol. 16, no. 2, pp. 1193–1226, 2019.

[4] R. O. A. de Lima, A. P. Bazo, D. M. F. Salvadori, C. M. Rech, D. de Palma Oliveira, and G. de Aragão Umbuzeiro, "Mutagenic and carcinogenic potential of a textile azo dye processing plant effluent that impacts a drinking water source," *Mutation Research/Genetic Toxicology and Environmental Mutagenesis*, vol. 626, no. 1-2, pp. 53–60, 2007.

[5] N. Selvakumar, F. Rahman, S. Rajasekaran, P. R. Narayanan, and T. R. Frieden, "Inefficiency of 0.3% carbol fuchsin in Ziehl-Neelsen staining for detecting acid-fast Bacilli," *Journal of Clinical Microbiology*, vol. 40, no. 8, pp. 3041–3043, 2002.

[6] K. Rl, V. Deshpande, and A. J. Iafrate, "General principles in the diagnosis of infection," *Diagnostic Pathology of Infectious Disease*, vol. 3, 2018.

[7] Y. Weldu, D. Asrat, Y. Woldeamanuel, and A. Hailesilasie, "Comparative evaluation of a two-reagent cold stain method with Ziehl-Nelseen method for pulmonary tuberculosis diagnosis," *BMC Research Notes*, vol. 6, no. 1, p. 323, 2013.

[8] B. K. Aziz and M. A. H. Karim, "Efficient catalytic photodegradation of methylene blue from medical lab wastewater using MgO nanoparticles synthesized by direct precipitation method," *Reac Kinet Mech Cat*, vol. 128, no. 2, pp. 1127–1139, 2019.

[9] M. F. Attallah, I. M. Ahmed, and M. M. Hamed, "Treatment of industrial wastewater containing Congo red and naphthol green B using low-cost adsorbent," *Environmental Science and Pollution Research*, vol. 20, no. 2, pp. 1106–1116, 2013.

[10] C. Namasivayam and D. J. S. E. Arasi, "Removal of Congo red from wastewater by adsorption onto waste red mud," *Chemosphere*, vol. 34, no. 2, pp. 401–417, 1997.

[11] A. El Gaidoumi, A. Arrahli, A. Loqman, F. Baragh, B. El Bali, and A. Kherbeche, "Efficient sol-gel nanocomposite TiO_2-clay in photodegradation of phenol: comparison to Labe-made and commercial photocatalysts," *Silicon*, vol. 14, no. 10, pp. 5401–5414, 2022.

[12] T. Adane, A. T. Adugna, and E. Alemayehu, "Textile industry effluent treatment techniques," *Journal of Chemistry*, vol. 2021, Article ID 5314404, 14 pages, 2021.

[13] A. Ghaly, R. Ananthashankar, M. Alhattab, and V. Ramakrishnan, "Production, characterization and treatment of textile effluents: a critical review," *Journal of Chemical Engineering & Process Technology*, vol. 5, no. 1, pp. 1–19, 2014.

[14] M. Ahmaruzzaman and V. K. Gupta, "Rice husk and its ash as low-cost adsorbents in water and wastewater treatment," *Industrial and Engineering Chemistry Research*, vol. 50, no. 24, pp. 13589–13613, 2011.

[15] M. K. Uddin and A. Nasar, "Walnut shell powder as a low-cost adsorbent for methylene blue dye: isotherm, kinetics, thermodynamic, desorption and response surface methodology examinations," *Scientific Reports*, vol. 10, no. 1, p. 7983, 2020.

[16] S. Akhouairi, H. Ouachtak, A. A. Addi, A. Jada, and J. Douch, "Natural sawdust as adsorbent for the Eriochrome Black T dye removal from aqueous solution," *Water, Air, & Soil Pollution*, vol. 230, no. 8, 2019.

[17] H. A. Ahsainea, M. Zbairb, and R. El Haoutia, "Mesoporous treated sewage sludge as outstanding low-cost adsorbent for cadmium removal," *Desalination and Water Treatment*, vol. 85, pp. 330–338, 2017.

[18] C. H. Weng and Y. F. Pan, "Adsorption of a cationic dye (methylene blue) onto spent activated clay," *Journal of Hazardous Materials*, vol. 144, no. 1-2, pp. 355–362, 2007.

[19] Y. C. Wong, Y. S. Szeto, W. H. Cheung, and G. McKay, "Adsorption of acid dyes on chitosan–equilibrium isotherm analyses," *Process Biochemistry*, vol. 39, no. 6, pp. 695–704, 2004.

[20] K. Kadirvelu, M. Kavipriya, C. Karthika, M. Radhika, N. Vennilamani, and S. Pattabhi, "Utilization of various agricultural wastes for activated carbon preparation and application for the removal of dyes and metal ions from aqueous solutions," *Bioresource Technology*, vol. 87, no. 1, pp. 129–132, 2003.

[21] M. S. Salman, M. N. Hasan, K. T. Kubra, and M. M. Hasan, "Optical detection and recovery of Yb(III) from waste sample using novel sensor ensemble nanomaterials," *Microchemical Journal*, vol. 162, article 105868, 2021.

[22] M. R. Awual, "A novel facial composite adsorbent for enhanced copper(II) detection and removal from wastewater," *Chemical Engineering Journal*, vol. 266, pp. 368–375, 2015.

[23] M. S. Salman, H. Znad, M. N. Hasan, and M. M. Hasan, "Optimization of innovative composite sensor for Pb(II) detection and capturing from water samples," *Microchemical Journal*, vol. 160, article 105765, 2021.

[24] A. Tor and Y. Cengeloglu, "Removal of Congo red from aqueous solution by adsorption onto acid activated red mud," *Journal of Hazardous Materials*, vol. 138, no. 2, pp. 409–415, 2006.

[25] T. Robinson, B. Chandran, and P. Nigam, "Removal of dyes from a synthetic textile dye effluent by biosorption on apple pomace and wheat straw," *Water Research*, vol. 36, no. 11, pp. 2824–2830, 2002.

[26] N. Basci, E. Kocadagistan, and B. Kocadagistan, "Biosorption of copper (II) from aqueous solutions by wheat shell," *Desalination*, vol. 164, no. 2, pp. 135–140, 2004.

[27] B. K. Aziz, "The impact of acidic spring water on Gwrgay natural clay and its adsorption efficiency: a kinetic, equilibrium and thermodynamic comparison," *Reaction Kinetics, Mechanisms and Catalysis*, vol. 133, no. 1, pp. 467–481, 2021.

[28] K. A. Babakr and B. K. Aziz, "Adsorptive removal of methyl orange from aqueous solutions with natural Garmak clay as cheap and efficient adsorbent in batch and continuous systems," *Journal of Zankoy Sulaimani - Part A*, vol. 21, no. 2, pp. 183–200, 2019.

[29] H. R. Ahmed, S. J. Raheem, and B. K. Aziz, "Removal of Leishman stain from aqueous solutions using natural clay of Qulapalk area of Kurdistan region of Iraq," *Science*, vol. 3, no. 3, pp. 165–175, 2017.

[30] B. K. Aziz, D. M. S. Salh, S. Kaufhold, and P. Bertier, "The high efficiency of anionic dye removal using Ce-Al13/pillared clay from Darbandikhan natural clay," *Molecules*, vol. 24, no. 15, p. 2720, 2019.

[31] M. Ahrouch, J. M. Gatica, K. Draoui, and H. Vidal, "Adding value to natural clays as low-cost adsorbents of methylene blue in polluted water through honeycomb monoliths manufacture," *Applied Sciences*, vol. 1, no. 12, pp. 1–14, 2019.

[32] W. A. Talavera-Pech, A. Ávila-Ortega, D. Pacheco-Catalán, P. Quintana-Owen, and J. A. Barrón-Zambrano, "Effect of functionalization synthesis type of amino-MCM-41 mesoporous silica nanoparticles on its RB5 adsorption capacity and kinetics," *Silicon*, vol. 11, no. 3, pp. 1547–1555, 2019.

[33] D. M. Salh, B. K. Aziz, and S. Kaufhold, "High adsorption efficiency of Topkhana natural clay for methylene blue from medical laboratory wastewater: a linear and nonlinear regression," *SILICON*, vol. 12, no. 1, pp. 87–99, 2020.

[34] R. Huang, Q. Liu, J. Huo, and B. Yang, "Adsorption of methyl orange onto protonated cross-linked chitosan," *Arabian Journal of Chemistry*, vol. 10, no. 1, pp. 24–32, 2017.

[35] Z. Aksu, "Determination of the equilibrium, kinetic and thermodynamic parameters of the batch biosorption of nickel(II) ions onto *Chlorella vulgaris*," *Process Biochemistry*, vol. 38, no. 1, pp. 89–99, 2002.

[36] I. Langmuir, "The adsorption of gases on plane surfaces of glass, mica and platinum," *Journal of the American Chemical Society*, vol. 40, no. 9, pp. 1361–1403, 1918.

[37] A. Shahat, K. T. Kubra, M. S. Salman, M. N. Hasan, and M. M. Hasan, "Novel solid-state sensor material for efficient cadmium(II) detection and capturing from wastewater," *Microchemical Journal*, vol. 164, article 105967, 2021.

[38] H. M. F. Freundlich, "Over the Adsorption in Solution," *The Journal of Physical Chemistry*, vol. 57, pp. 385–471, 1906.

[39] A. A. Khan and R. P. Singh, "Adsorption thermodynamics of carbofuran on Sn (IV) arsenosilicate in H^+, Na^+ and Ca^{2+} forms," *Colloids Surface*, vol. 24, no. 1, pp. 33–42, 1987.

[40] A. S. Ozcan and A. Ozcan, "Adsorption of acid dyes from aqueous solutions onto acid-activated bentonite," *Journal of Colloid and Interface Science*, vol. 276, no. 1, pp. 39–46, 2004.

[41] L. Cottet, C. A. P. Almeida, N. Naidek, M. F. Viante, M. C. Lopes, and N. A. Debacher, "Adsorption characteristics of montmorillonite clay modified with iron oxide with respect to methylene blue in aqueous media," *Applied Clay Science*, vol. 95, pp. 25–31, 2014.

[42] S. J. Tan, L. Liu, and J. W. Chew, "Competitive and synergistic adsorption of mixtures of polar and nonpolar gases in carbonaceous nanopores," *Langmuir*, vol. 37, no. 22, pp. 6754–6764, 2021.

[43] B. B. Mohammed, A. Hsini, Y. Abdellaoui et al., "Fe-ZSM-5 zeolite for efficient removal of basic fuchsin dye from aqueous solutions: synthesis, characterization and adsorption process optimization using BBD-RSM modeling," *Journal of Environmental Chemical Engineering*, vol. 8, no. 5, article 104419, 2020.

[44] M. El-Azazy, A. S. El-Shafie, A. Ashraf, and A. A. Issa, "Eco-structured biosorptive removal of basic fuchsin using pistachio nutshells: a definitive screening design—based approach," *Applied Sciences*, vol. 9, no. 22, p. 4855, 2019.

[45] W. Bessashiaa, Y. Berredjem, Z. Hattab, and M. Bououdina, "Removal of basic fuchsin from water by using mussel powdered eggshell membrane as novel bioadsorbent: equilibrium, kinetics, and thermodynamic studies," *Environmental Research*, vol. 186, article 109484, 2020.

[46] H. Qiao, Y. Zhou, F. Yu et al., "Effective removal of cationic dyes using carboxylate-functionalized cellulose nanocrystals," *Chemosphere*, vol. 141, pp. 297–303, 2015.

[47] C. Wang, C. Feng, Y. Gao, X. Ma, Q. Wu, and Z. Wang, "Preparation of a graphene-based magnetic nanocomposite for the removal of an organic dye from aqueous solution," *Chemical Engineering Journal*, vol. 173, no. 1, pp. 92–97, 2011.

[48] A. M. Awad, R. Jalab, A. Benamor et al., "Adsorption of organic pollutants by nanomaterial-based adsorbents: an overview," *Journal of Molecular Liquids*, vol. 301, article 112335, 2020.

[49] E. O. Oyelude, F. Frimpong, and D. Dawson, "Studies on the removal of basic fuchsin dye from aqueous solution by HCl treated malted sorghum mash," *Journal of Materials and Environmental Science*, vol. 6, no. 4, pp. 1126–1136, 2015.

[50] Y. H. Zhao, J. T. Geng, J. C. Cai, Y. F. Cai, and C. Y. Cao, "Adsorption performance of basic fuchsin on alkali-activated diatomite," *Adsorption Science & Technology*, vol. 38, no. 5–6, pp. 151–167, 2020.

[51] M. El Haddad, "Removal of basic fuchsin dye from water using mussel shell biomass waste as an adsorbent: equilibrium, kinetics, and thermodynamics," *Journal of Taibah University for Science*, vol. 10, no. 5, pp. 664–674, 2016.

[52] C. Li, Y. He, L. Zhou et al., "Fast adsorption of methylene blue, basic fuchsin, and malachite green by a novel sulfonic-grafted triptycene-based porous organic polymer," *RSC Advances*, vol. 8, no. 73, pp. 41986–41993, 2018.

[53] H. J. Lee and S. T. Ong, "Immobilization of rambutan (Nephelium lappaceum) peel as a sorbent for basic fuchsin removal," *Environment Protection Engineering*, vol. 43, p. 1, 2017.

[54] J. Yu, B. Li, X. Sun, J. Yuan, and R. Chi, "Poly(amic acid)-modified biomass of Baker's yeast for enhancement adsorption of methylene blue and basic magenta," *Applied Biochemistry and Biotechnology*, vol. 160, no. 5, pp. 1394–1406, 2010.